Combined Experimental and Computational Hydrostatic Compression Study of Crystalline Ammonium Perchlorate

Cite as:
Hunter, S., Davidson, A. J., Morrison, C. A., Pulham, C. R., Richardson, P., Farrow, M. J., Marshall, W. G., Lennie, A. R., & Gould, P. J. (2011). Combined Experimental and Computational Hydrostatic Compression Study of Crystalline Ammonium Perchlorate. *Journal of Physical Chemistry C*, 115 (38), 18782-18788.

Manuscript received: 08/02/2011; Accepted: 25/08/2011; Article published: 08/09/2011

Combined Experimental and Computational Hydrostatic Compression Study of Crystalline Ammonium Perchlorate**

Steven Hunter,[1] Alistair J. Davidson,[1,2] Carole A. Morrison,[1,*] Colin R. Pulham,[1,*] Patricia Richardson,[1] Matthew J. Farrow,[1] William G. Marshall,[3] Alistair R Lennie[4] and Peter J. Gould[5]

[1]EaStCHEM and Centre for Science at Extreme Conditions, School of Chemistry, Joseph Black Building, University of Edinburgh, West Mains Road, Edinburgh, EH9 3JJ, UK.

[2]Institute for Shock Physics, Washington State University, Pullman, Washington 99164-7041, United States.

[3]ISIS Neutron and Muon Facility, Rutherford Appleton Laboratory, Harwell Science and Innovation Campus, Didcot, Oxfordshire, OX11 0QX, UK.

[4]Diamond Light Source, Harwell Science and Innovation Campus, Didcot, Oxfordshire, OX11 0DE, UK.

[5]QinetiQ Bristol, Building 240, The Close, Bristol Business Park, Coldharbour Lane, Bristol, BS16 1FJ, UK.

[*]Corresponding author; C.A.M. e-mail: carole.morrison@ed.ac.uk; C.R.P. e-mail: c.r.pulham@ed.ac.uk

[**]We thank the Scottish Funding Council (SPIRIT) and QinetiQ (in support of MOD research) for contribution towards a studentship (S.H.); the STFC (Science & Technology Facilities Council) and EPSRC for contributions towards a studentship (A.J.D.); the STFC for the provision of neutron and X-ray beamtime; the EaStCHEM Research Computing Facility (http://www.eastchem.ac.uk/rcf) and the Edinburgh Compute and Data Facility (ECDF) (http://www.ecdf.ed.ac.uk/) for access to computing resources. Both computing facilities are partially supported by the eDIKT initiative (http://www.edikt.org.uk).

Supporting information:
Details of the 0.0 and 3.5 GPa experimental and computationally calculated structures, given as fractional coordinates of the unit cell for both OTF and 00PBE types of pseudopotential. Figures displaying the pressure dependence of lattice parameter and unit cell volume calculated using 00PBE pseudopotentials. Calculated equation of state parameters for 00PBE pseudopotential calculations. This material is available free of charge via the Internet at http://pubs.acs.org

Graphical abstract:

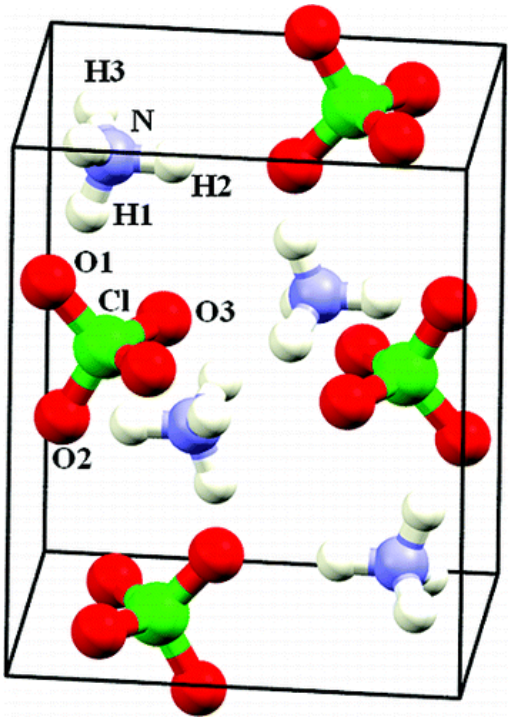

Abstract:

We have obtained detailed structural information for the energetic salt ammonium perchlorate (AP) at pressures up to ~8 GPa through a combination of X-ray and neutron diffraction. Under hydrostatic conditions, AP undergoes a first-order phase transition at 3.98(5) GPa, broadly consistent with results from previous studies. We have successfully solved and refined the structure of the new orthorhombic phase (phase II, space group*Pnma*), which features a more close-packed structure with more extensive hydrogen bonding than the polymorph obtained at ambient pressure (phase I). Equations of state have been obtained for phase I from 0 to 3.5 GPa and for the new phase 4 to 8.1 GPa. To complement these experimental studies, we have also performed density functional theory (DFT) calculations of the hydrostatic compression of AP in the region of 0.0–3.5 GPa. A comparison of the performance of different pseudopotentials and DFT dispersion correction schemes in calculating crystal geometries at high pressure has been performed. The results highlight the fact that care must be taken when choosing pseudopotentials for high-pressure studies and that no significant improvements in the calculation of crystal geometries of AP are obtained by employing DFT-D corrections.

1. Introduction

Energetic materials are defined as those that release heat and, generally, gaseous products upon stimulus by heat, impact, shock, spark, *etc*.[1] The performance of energetic materials can depend on a number of factors that include: sensitivity to detonation by stimulus, the detonation velocity, the chemical reactivity, the thermal stability, and crystal density. Polymorphism and solid-state phase transitions in these materials may therefore have significant consequences and the performance of an energetic formulation may be highly dependent on the particular polymorph that is used.

The effective modeling of the characteristics and performance of solid energetic materials under operational conditions therefore requires detailed knowledge of the crystal structures and properties of these compounds. In many cases it is the crystal structure of the compound under ambient conditions that is used as the basis for modeling properties at higher temperatures and pressures, for the simple reason that structural information under more extreme conditions of pressure and temperature is often not available. However, it is well known that extreme conditions can lead to substantial changes in intermolecular interactions and molecular geometries, and can even induce phase transitions.

Ammonium perchlorate (AP) is an energetic oxidizer that is widely used in solid rocket motors.[2,3,4] At ambient pressure and temperature, AP crystallizes in the orthorhombic crystal system, space group *Pnma* (see **Figure 1**). Variable temperature studies indicate that, at least up to 78 K, the ammonium ions undergo increasingly large amplitude rotational oscillations about definite equilibrium positions such that they exhibit essentially free rotation.[2,3,4] On heating to above 511-

513 K, a reversible phase transition to a cubic structure has been observed in which there is almost unrestricted rotational reorientation of the perchlorate ions.[5]

By contrast, the structural behavior of AP at high pressures is relatively poorly understood and several studies in the literature appear to contradict each other. The first high-pressure study by Bridgman identified a very small change in volume at 3.1 GPa when a sample of AP was subjected to shear experiments at elevated temperatures.[6] The orthorhombic-to-cubic transition that occurs at 511 K at ambient pressure has been followed as a function of pressure up to 0.4 GPa, and this study reported a very strong pressure dependence (216 K GPa^{-1}) of the transition,[7] but subsequent optical studies determined that it was only weakly pressure-dependent.[8] These studies also reported the pressure dependence of the solid-liquid transition and claimed that there was no evidence for a high-pressure phase transition up to 26 GPa.[8] A powder X-ray diffraction study up to 5.0 GPa, combined with a shock compression study of the bulk speed of sound, identified no discernible phase changes up to 3.57 GPa, but by 4.70 GPa some alteration in the diffraction pattern was observed which was indicative of a phase transition. The new diffraction pattern, however, proved impossible to index.[9] An infrared study by Brill *et al*. noted the disappearance of the vibrational band at 939 cm^{-1} associated with the ν_1 mode of the ClO_4^- group at pressures between 1.0-2.4 GPa, and tentatively assigned this to the orthorhombic-to-cubic phase transition.[10] The response of single crystals of AP to shockwaves up to 6.2 GPa has also been studied but under these conditions no features were observed that could be identified as a shock-induced, sustained chemical reaction or phase transformation.[11] A subsequent study used these data to construct a thermo-mechanical model for shock compression normal to the (210) and (001) crystal planes and suggested that any phase transition occurred either with a negligible change in volume or with very slow kinetics.[12] In the most thorough study to date, Peiris *et al*. investigated the effects of pressures up to 5.6 GPa on AP

using powder X-ray diffraction and infrared and Raman spectroscopy.[13] Discontinuities observed in the Raman spectra at pressures of approximately 0.9 GPa and 3.0 GPa were attributed to phase transitions. New peaks were also observed in the X-ray diffraction pattern above 0.9 GPa that could not be indexed to the orthorhombic structure. The intensities of these new peaks increased up to 2.9 GPa, but above 3.0 GPa all of the peaks observed at lower pressure disappeared completely and a new set of peaks appeared that persisted up to 5.6 GPa, the limit of the study. Unfortunately, the authors were unable to index either of the patterns associated with the new high-pressure phases. The pressure-volume data up to 2.9 GPa obtained from the X-ray measurements were used to calculate a bulk modulus of 16.0 ± 0.2 GPa.[13] Thus, to summarize, there are numerous conflicting accounts in the literature concerning the high pressure behavior of AP, clearly demonstrating that a definitive study of the high pressure behavior of AP is now needed.

A complementary approach to experiment is atomistic simulation. Simulations can provide an effective way to model the properties and structures of crystalline materials. Zhu *et al.* recently performed an ambient-pressure DFT study of AP[14], followed up by a hydrostatic compression study.[15] However, we note that the authors used the incorrect crystal structure for their computational model – the structure with space group $Pna2_1$ was used rather than the *Pnma* structure. For this reason we have performed new calculations on AP, and also take this opportunity to benchmark the performance of two different types of pseudopotential and a number of different DFT dispersion correction schemes under an applied external pressure. Although AP is an ionic material, and therefore the contribution towards intermolecular bonding from dispersion may be expected to be quite low, the ions are linked through a hydrogen bond network, and thus the effect is

worthy of investigation.[16,17] As this work involves calculations at high pressure, the choice of pseudopotential is an important factor to consider in the simulations.

To summarize, we have used a combination of X-ray and neutron diffraction techniques to study AP, and have obtained detailed structural information for this material at pressures up to approximately 8 GPa. We report the crystal structure of the previously observed high-pressure phase, hereby denoted as phase II. In addition, computational studies of the hydrostatic compression of AP have been performed in the region of 0-3.5 GPa to compare the performance of different pseudopotentials and to benchmark recently developed DFT dispersion correction schemes (DFT-D) in calculating crystal geometries at high pressure.

The organization of the paper is as follows. In Section 2 we describe the experimental techniques used to obtain detailed structural information at pressures up to approximately 8 GPa and provide specific details of the computational parameters used in calculations. The results of the experimental compression study are presented in Section 3, along with a comparison of the results obtained by different computational DFT-D schemes and types of pseudopotentials. The main conclusions of this work are summarized in Section 4.

2. Experimental and computational methods

2.1 Sample preparation. Samples of AP were obtained from Sigma-Aldrich. Full deuteration of the material was obtained by repeated crystallization from D_2O (99.9 at%, Sigma-Aldrich) under dry N_2.

2.2 Neutron powder diffraction studies. A lightly ground sample (*ca.* 100 mg) of AP was loaded into an encapsulated TiZr gasket,[18] together with a small quantity of 4:1 perdeuterated methanol/ethanol as a pressure-transmitting medium (PTM) and a small quantity of sodium chloride to act as a pressure calibrant. The resulting capsule assembly was then compressed within a type V3b Paris-Edinburgh (P-E) press[19] equipped with standard single toroid anvils with cemented WC cores (Ni binder). The P-E press ram pressure was monitored and varied by means of a computer controlled hydraulic system. High-pressure neutron powder diffraction data for AP were collected using the PEARL/HiPr diffractometer at the UK spallation neutron source, ISIS, located at the STFC Rutherford Appleton Laboratory. Time-of-flight (TOF) neutron powder diffraction data suitable for structure refinement were obtained by electronically focusing the individual detector element spectra from the PEARL/HiPr $2\theta=90°$ detector banks. The resulting summed pattern was then normalized with respect to the incident beam monitor and the scattering from a standard vanadium calibration sample. Lastly, the diffraction pattern intensity scale was corrected for the wavelength and scattering-angle dependence of the neutron attenuation by the anvil (WC) and gasket (TiZr) materials. Full-profile Rietveld refinements of the TOF neutron powder diffraction patterns were carried out using the GSAS package.[20] Sample pressures were calculated from the refined NaCl lattice parameters and the room-temperature equation of state for NaCl as derived by Decker[21] with an uncertainty of ± 0.05 GPa. Data collection times per pressure point ranged between 1 and 6 hours at an equivalent of 165 μA ISIS proton current.

2.3 X-ray Diffraction studies. High-pressure X-ray experiments were performed using a Merrill-Bassett diamond anvil cell (40° half-opening angle),[22] equipped with 600 μm culets and a tungsten gasket with a 300 μm hole. A 4:1 mixture of methanol/ethanol or HT-70 was used as a hydrostatic

PTM. A small ruby chip was also loaded into the cell as the pressure calibrant, with the ruby fluorescence method being utilized to measure the pressure.[23] Single crystal diffraction data were collected on Station 16.2SMX and powder diffraction data were collected on Station 9.5HPT at the CCLRC Daresbury Laboratory, UK.

2.5 Computational methods. Structure optimizations (at ambient pressure and under hydrostatic externally applied pressure conditions) were performed using density functional theory (DFT) and the plane-wave pseudopotential method as implemented in CASTEP version 5.5,[24] utilizing the dispersion correction schemes of Grimme[25] and Tkatchenko & Scheffler.[26] Treatment of electronic exchange and correlation was handled by the generalized gradient approximations (GGA) formalized by Perdew, Burke and Ernzerhof (PBE).[27] We tested the performance of two different types of pseudopotential [Vanderbilt 00PBE,[28] and on-the-fly (OTF)[29]]; the plane-wave cutoff energy used throughout was 650 eV, which ensured that total energies were converged to less than 5 meV per unit cell for both types of pseudopotential. Brouillon zone sampling was obtained using a $2 \times 3 \times 3$ (4 k-point) Monkhorst-Pack[30] grid. The structure was relaxed [using the Broyden, Fletcher, Goldfarb and Shannon (BFGS)[31] method] to allow both atomic coordinates and unit cell vectors to optimize simultaneously while constraining space group geometry (convergence criteria: maximum change in system energy = 2×10^{-5} eV, maximum root-mean-square (RMS) force = 0.01 eV Å^{-1}, maximum RMS stress = 0.01 GPa and maximum RMS displacement = 0.002 Å). Following successful geometry optimization, external hydrostatic pressures were applied from 0 – 3.5 GPa, in 0.5 GPa increments.

3. Results and discussion

3.1 Crystallographic data. The sequence of powder neutron diffraction patterns obtained for $ND_4^+ClO_4^-$ as a function of pressure is shown in **Figure 2**, where the order of patterns (from bottom to top) reproduces the order in which they were collected on PEARL/HiPr. Up to 3.49(5) GPa the powder patterns can be indexed to the ambient pressure form, phase I. A smooth decrease in volume from 399.09 $Å^3$ (at 0.01(5) GPa) to 346.50 $Å^3$ (at 3.49(5) GPa) was observed, which corresponds to an increase in density of *ca.* 13.2 %. The unit-cell volume can be fitted to a 3rd order Birch-Murnaghan[32] equation of state. The two key parameters in this fit are B_0 (the bulk modulus, which describes how compressible the crystal structure is over the pressure range studied), and B' (the first derivative of the bulk modulus, which describes the curvature of the compression curve). The values obtained were B_0 = 14.91(25) GPa, and B' = 7.32(23); this is in good agreement with studies of AP by Peiris *et al*.[13] (based on data collected up to 2.9 GPa), and by Sandstrom *et al*.[9]

Rietveld refinements of the diffraction patterns were performed using the GSAS[20] program, using the following constraints and restraints: the geometries of the ND_4^+ and ClO_4^- ions were fixed as regular tetrahedra, and the N-D and Cl-O bonds were loosely restrained to be 1.03 and 1.44 Å, respectively. **TABLE 1** lists the lattice parameters obtained from Rietveld refinements, additionally fitting statistics, wR_p and χ^2 are listed for each pressure. At 0.01(5) GPa each perchlorate ion is surrounded by seven ammonium ions and each ammonium ion is surrounded by seven perchlorate ions, with the N...O distances of all neighbors lying within 3.20 Å. The O1 and O3 atoms each form three hydrogen bonds (< 2.70 Å) to neighboring ammonium ions, while O2 forms only one hydrogen bond with D1 at a distance of 1.98(2) Å. As pressure increases we observe no significant changes to the structure other than the cations and anions moving closer together, thereby reducing

the sizes of the voids in the structure. At 3.49(5) GPa we observe all seven N...O neighbor distances to lie within 3.04 Å. The isotropic displacement parameters (u_{iso}) associated with the deuterium atoms become progressively smaller as pressure increases, indicating that the essentially free rotation observed under ambient conditions becomes more restricted, thus mirroring the effects of cooling. Even at 3.49(5) GPa, however, it is clear that the deuterium atoms of the ammonium ions are still undergoing substantial motion about their equilibrium positions.

At a pressure of 3.98(5) GPa, the diffraction pattern was observed to become significantly more complex, with the appearance of new peaks in addition to those associated with phase I. This suggests the presence of a new phase. On increasing the pressure to 4.60(5) GPa, the Bragg peaks associated with phase I disappeared completely to give a pattern that could be indexed to a new orthorhombic unit cell, corresponding to a high-pressure phase which we denote here as phase II. This phase persisted up to 8.13(5) GPa, which was the maximum pressure of the study.

The responses of the three lattice vectors and the overall cell volume to pressure are shown in **Figure 3**. This figure includes data points recorded on both compression and decompression. Across the phase I-II transition, the *a*-axis cell parameter decreases, *b* increases, and *c* remains largely unchanged, resulting in a net decrease in unit-cell volume of 6.1 $Å^3$ (1.8 %). From 3.98(5) to 8.13(5) GPa the *a*-, *b*-, and *c*-axes decrease further by 3.8 %, 1.8 %, and 3.1 %, respectively. The associated increase in density over this pressure range is 8.6 %. Fitting a 3rd order Birch-Murnaghan[32] equation of state to the pressure/volume response in this region yields parameters of B_0 = 22.4(26) GPa, and B' = 4.4(5), indicating that the high-pressure phase is significantly less compressible than phase I. On the basis of systematic absences in the diffraction pattern, the space

group of phase II was tentatively assigned as *Pnma*, although $P2_12_12_1$ was an alternative possibility. In order to resolve this, a single crystal X-ray diffraction experiment was performed in which a single crystal of AP was progressively compressed. The single crystal survived the transition intact and data collected at 4.3 GPa could be indexed to the high-pressure orthorhombic cell and the space group was identified unequivocally as *Pnma*. Refinements of the diffraction patterns obtained for the high-pressure phase employed the same restraints as used for refinements of phase I with the Rietveld refinement of the neutron powder diffraction pattern shown in **Figure 4**. The pattern recorded at 3.98(5) GPa could then be satisfactorily fitted to a mixture of phases I and II. This allows direct comparison of the molecular volumes for each phase and clearly demonstrates that phase II is 1.8 % more dense than phase I at this pressure and confirms that the phase transition is first order. This is also apparent in a space-fill comparison of the two phases shown in **Figure 5**. Here it can be seen that as pressure is applied to the phase I structure the central void becomes smaller; upon transformation to phase II the more efficient packing virtually eliminates this central void. For both phases I and II, the N-D and Cl-O distances are essentially unchanged - this behavior is typical for molecular species in this pressure regime. However, one of the consequences of the more efficient packing in phase II is the formation of a short O…D contact (1.78 Å).

On slow decompression of the sample the high-pressure phase persisted to 3.82(5) GPa and by the next pressure point at 2.76(5) GPa, the sample had completely transformed back to phase I. No evidence for any other crystalline phases was observed and this rules out the possibility of sample decomposition or reaction with the pressure-transmitting fluid during the course of the experiment.

The results of this study shed some light on the findings of previous studies which have suggested that AP undergoes a phase transition in the range 3.1-4.7 GPa with a relatively small volume change. The differences in reported transition pressure between the present study and other studies might be attributed to the fact that our neutron study used perdeuterated ammonium perchlorate. However, this is clearly not the reason in this case because the transition pressures for the X-ray diffraction experiments (using NH_4ClO_4) and the neutron diffraction experiments (using ND_4ClO_4) are very similar. A more likely explanation lies in the rather different conditions under which each study has been performed. Several shock-wave studies have suggested that there is no pressure-induced phase transition, or if there is, that it either involves a small volume change or is kinetically slow under the conditions of the experiment.[9,11,12] Our studies have shown that the volume change associated with the phase transition is indeed small. Perhaps the most important variable in isothermal direct compression experiments is the choice of pressure-transmitting medium. We deliberately chose to use 4:1 methanol/ethanol as the medium in these experiments on account of it remaining truly hydrostatic up to *ca.* 9 GPa,[33] despite the potential risk of reaction with the sample. Past experience involving compression of relatively soft organic compounds has shown that pressure-induced phase transitions can be inhibited when fluids such as Fluorinert FC-75 become non-hydrostatic. Although higher pressures have been claimed, careful studies by Varga *et al*. on the effect of pressure on the line-width of the (101) reflection of a quartz crystal demonstrated that Fluorinert FC-75 remains truly hydrostatic only up to 1.2 GPa.[33] Conversely, there may also be occasions when non-hydrostatic behavior causes shear stresses that can *induce* phase transitions, such as reported for ammonium nitrate.[34,35] Bridgman's transition pressure of 3.1 GPa involved the application of non-hydrostatic shear stresses at elevated temperatures,[6] and so these conditions are also very different from those used in the current study. The study by Peiris *et al*.[13] is the one that

involves conditions closest to our own. Using energy dispersive powder X-ray diffraction and either sodium chloride or Fluorinert FC-75 as a pressure-transmitting medium, the authors observed changes in intensities over the range 2.9-3.3 GPa, and the appearance of a new pattern above 3.3 GPa. The rather lower transition pressure in the earlier study is presumably a consequence of the non-hydrostatic conditions associated with the use of NaCl or FC-75 as the pressure-transmitting medium.[33] Comparison of these published patterns with those calculated from our structure of phase II indicates that at least some of the peaks attributable to phase II are present, although there are some significant differences in intensity as well as some additional peaks. The origin of these additional peaks is not obvious, although it is of course possible that non-hydrostatic conditions may induce a transition to a different phase. It is also possible that the high intensity X-ray beam used in the energy dispersive experiments may have induced partial decomposition of the sample – AP is known to be susceptible to irradiation with X-rays and γ-rays leading to the formation of radical species[36] and plastic deformation of crystals,[37] and both of these phenomena might also encourage other phase transitions.

3.2 Computational Results

3.2.1 Crystal geometries. A comparison between the performance of conventional DFT and DFT-D for unit cell optimization was performed by considering three different correction schemes: (i) no dispersion correction (NDC), (ii) the dispersion correction developed by Grimme[25] (G06) and (iii) the dispersion correction developed by Tkatchenko & Scheffler[26] (TS). Compression studies in the region 0.0–3.5 GPa were performed allowing atomic positions and unit cell vectors to optimize while preserving crystal symmetry. All data displayed in the figures and tables in the main text

relate to calculations performed using the OTF pseudopotentials. Data relating to the calculations performed using the 00PBE pseudopotentials are logged in the Supplementary Information.

The effect of pressure on the lattice parameters *a*-, *b*- and *c*- for the three DFT schemes is shown in **Figure 6**. From this, it can be seen that all calculations underestimate the ambient pressure *a*-axis lattice parameter, NDC by 2.7 %, TS by 5.8 % and G06 by 5.6 % (with the corresponding values for the 00PBE pseudopotentials being 2.9, 6.0 and 5.8 %). As pressure is applied the *a*-axis lattice parameter decreases monotonically for both types of pseudopotential, which follows the experimental trend. The OTF pseudopotentials show a steady compression rate, in contrast to the 00PBE pseudopotentials which tended towards more erratic predictions in the pressure region 1.0-2.5 GPa for all three DFT schemes. However, regardless of how favorable the compression trend is, both types of pseudopotential produce similar overall compression parameters between 0.0–3.5 GPa. Experimentally the compression ratio at 3.5 GPa, a/a_0 (where a_0 is the length of unit cell parameter *a* at 0 GPa) is 0.944; computationally NDC provides a/a_0 = 0.939, TS = 0.953 and G06 = 0.951 (with the corresponding values for the 00PBE pseudopotentials being 0.932, 0.947 and 0.946).

In contrast to the *a*-axis, all three functionals overestimate the *b*-axis lattice parameter: NDC overestimates the *b*-axis by 9.9 %, TS by 7.6 % and G06 by 4.7 % at ambient pressure (with the corresponding values for the 00PBE pseudopotentials being 10.0, 7.7 and 4.9 %). As expected from experiment, the *b*-axis lattice parameter decreases monotonically for both types of pseudopotential. As in the case of the *a*-axis the OTF pseudopotentials replicate the trend of smooth compression set by experiment, while the 00PBE pseudopotentials deviate from the predicted trend. The experimental compression ratio of the *b*-axis at 3.5 GPa, b/b_0 is 0.967; NDC = 0.948, TS = 0.963

and G06 = 0.976 (with the corresponding values for the 00PBE pseudopotentials being 0.952, 0.967 and 0.977).

For the compression of the *c*-axis with respect to pressure, the two dispersion corrections underestimate the *c*-axis lattice parameter. Using OTF pseudopotentials at ambient pressure, the difference between calculated and experimental *c*-axes are 0.0 % using NDC, -1.8 % for TS and -3.0 % using the G06 scheme (with the corresponding values for the 00PBE pseudopotentials being 0.1, -1.9 and -3.1 %). Analogous results to the *a*- and *b*-axes were obtained for the *c*-axis apropos compression trends. The experimental percentage compression c/c_0 = 0.952, NDC = 0.952, TS = 0.965 and G06 = 0.962 (with the corresponding values for the 00PBE pseudopotentials being 0.953, 0.965 and 0.964).

Thus, to summarize, while the overall lattice vectors produce average errors of approximately 5 %, the prediction for the rate of compression is much better; values obtained for the compression of all lattice vectors are within 2 % of experimental values between 0.0–3.5 GPa.

Figure 7 depicts the overall unit cell volume compression as a function of pressure. The compression results are compared against experiment and are fitted to 3rd order Birch-Murnaghan equations of state.[32] The results indicate that at ambient pressure, the unit cell volumes differ from experiment by +7.0 %, -0.4 % and -4.2 % for NDC, TS and G06 respectively (with the corresponding values for the 00PBE pseudopotentials being +7.0, -0.6 and -4.3 %). Looking at these unit cell volumes alone, it seems that the TS dispersion correction provides a very good model, nonetheless a good computational model must accurately describe not only the cell size but also the

cell shape. The TS functional attains this favorable unit cell volume by significantly underestimating the *a*-axis and overestimating the *b*-axis, thereby predicting the 'correct' unit cell volume by a cancellation of errors.

As the degree of compression was increased the inaccuracy of the predicted unit cell volume diminished using NDC. These results mirror those obtained by Byrd *et al*.[38] and Conroy *et al.*[39] who concluded that as the degree of compression is increased, the intermolecular interactions are enhanced and thus conventional DFT is better able to accurately describe the intermolecular interactions to provide a better agreement with experiment.

An appropriate way to compare the simulated compression of the overall unit cell (*i.e.* both cell shape and volume) with experiment is to calculate an equation of state. It can be seen in **TABLE 2** that the NDC strategy provides the best agreement with experiment for both B_0 and B'. Although the curvature of the equations of state predicted by TS and G06 models are respectable, both significantly overestimate the bulk modulus.

3.2.2 Internal Geometries In all simulations all N-H and Cl-O bond lengths, and H-N-H and O-Cl-O bond angles are well within 2 % of the experimental values, demonstrating no superiority between either type of pseudopotential or choice of DFT-D scheme under ambient or elevated pressure conditions.

4. Conclusions

Advances in the techniques for the collection and analysis of high-pressure data are now enabling accurate determination of structures of energetic materials under extreme conditions. Ammonium perchlorate has been studied using high-pressure diffraction techniques, and for the first time structural information at the molecular level has been obtained at elevated pressures, including the structure solution and refinement of a new high-pressure phase of ammonium perchlorate, denoted here as phase II. Comparisons with previous experimental studies highlight the importance of hydrostatic and non-hydrostatic conditions on the occurrence of phase transitions.

In addition, density functional theory studies of the hydrostatic compression of AP have been performed in the region of 0.0-3.5 GPa, comparing the performance of different pseudopotentials and DFT dispersion correction schemes in calculating crystal geometries at high pressure. The results demonstrate that the choice of pseudopotential used for high pressure calculations is important, highlighting that 00PBE ultrasoft pseudopotentials although accurate at ambient pressure are unable to accurately describe the high-pressure behavior of AP. Using 'on-the-fly' pseudopotentials generated using the CASTEP code reproduces the experimental compression behavior of phase I AP for all DFT dispersion correction schemes used. This study has established that no significant improvement in the calculation of crystal geometries of ammonium perchlorate is obtained by employing DFT-D corrections. It has also highlighted that as the applied pressure increases, the need for DFT-D correction diminishes, which is in accordance with previous findings.

7. Figure Captions

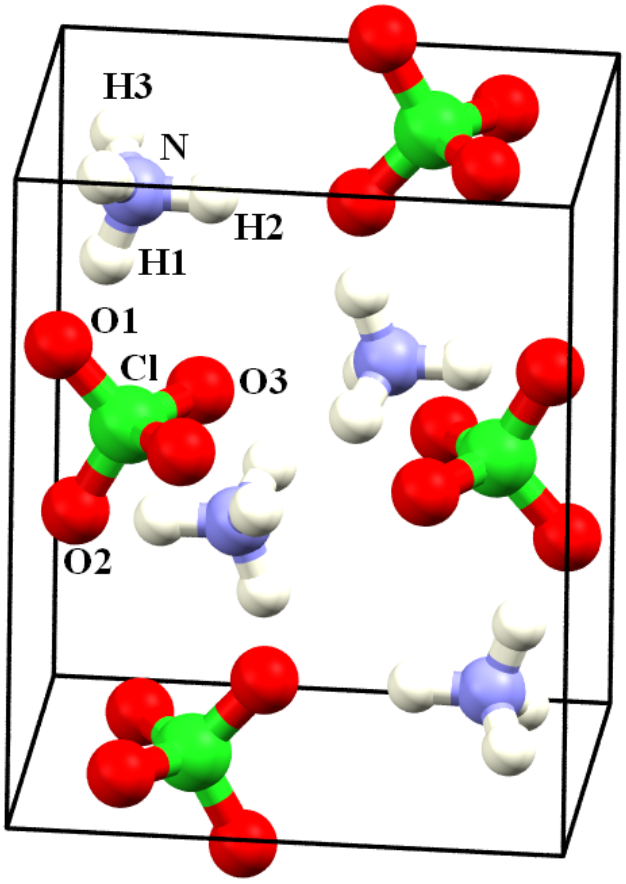

Figure 1 Unit cell for ammonium perchlorate at ambient pressure (phase I).

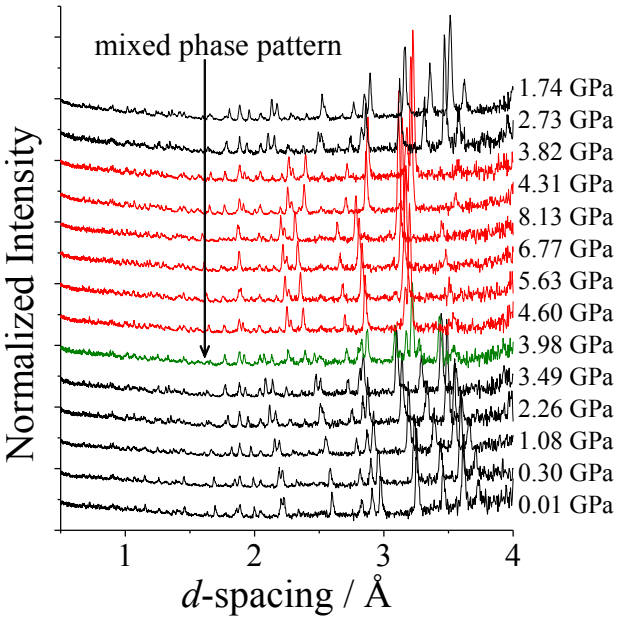

Figure 2 Sequence of neutron powder diffraction patterns obtained for ND_4ClO_4. Patterns indexed to phase I are shown in black, phase II in red and the mixed phase at 3.98 GPa is shown in green.

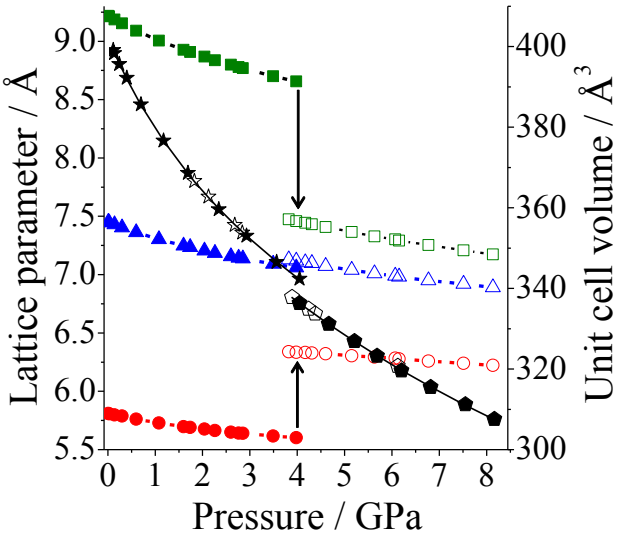

Figure 3 Variation of lattice parameters and unit cell volume of ND_4ClO_4 with pressure. —■— *a*- , —●— *b*- and, —▲— *c*- vectors (solid phase I, open phase II). ★ phase I, ⬟ phase II (solid compression, open decompression), ▬ phase I and phase II 3rd order Birch-Murnaghan equation of state fits. Phase I equation of state parameters: V_0 = 399.33(20) Å^3, B_0 = 14.91(25) GPa, B' = 7.32(23). Phase II equation of state parameters: V_0 = 384.1(3.2) Å^3, B_0 = 22.4(2.6) GPa, B' = 4.36(53).

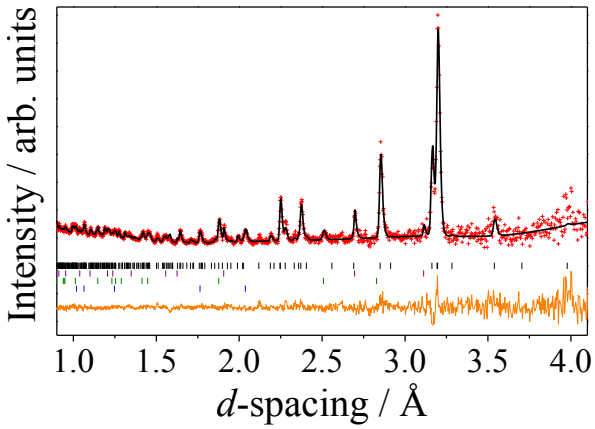

Figure 4 Rietveld refinement of neutron powder diffraction pattern collected at 4.60 GPa using AP structural model (black tick marks), along with the Pb pressure marker (purple tick marks) and the diffracted intensities from the WC anvils and Ni binder (green and blue tick marks respectively). The experimental data (I_{obs}) are represented as red crosses, the calculated pattern (I_{calc}) is shown in black and the difference (I_{obs} - I_{calc}) in orange.

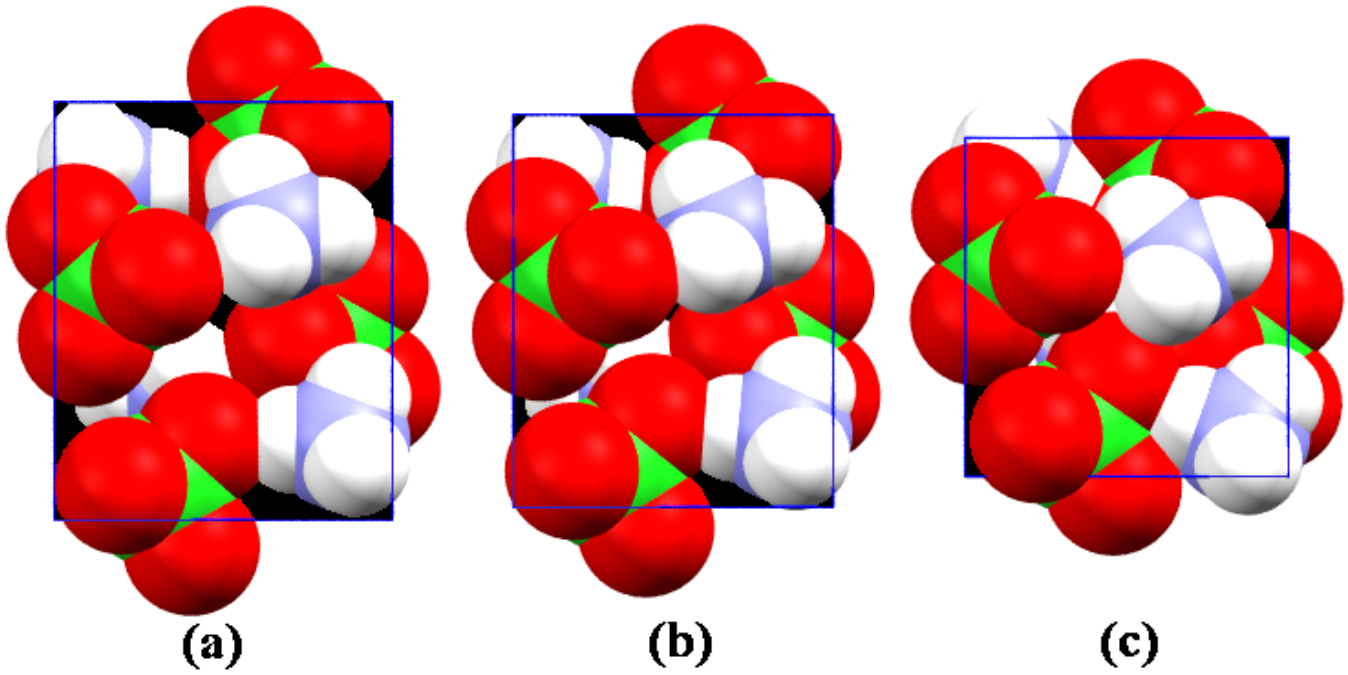

Figure 5 Space-fill representation of (a) ambient pressure (phase I), (b) 3.98 GPa (phase I) and (c) 3.98 GPa (phase II) structures.

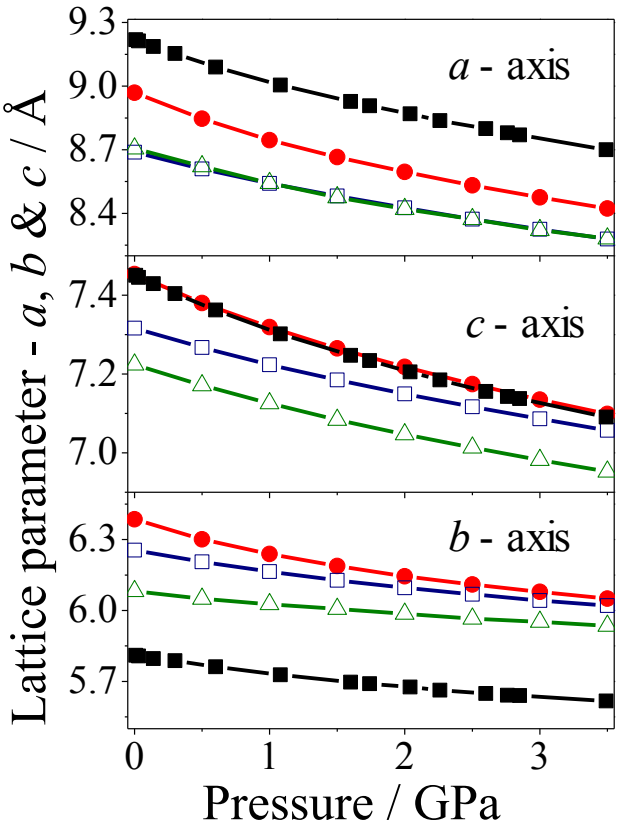

Figure 6 Lattice parameters as a function of hydrostatic pressure for crystalline AP. NDC —●—, TS —□—, G06 —Δ— and experimental (this work) —■—.

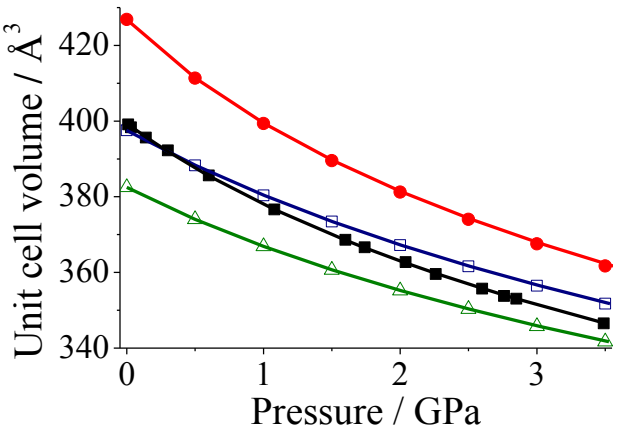

Figure 7 Unit cell volume as a function of pressure fitted with 3rd order Birch-Murnaghan equations of state for crystalline AP. NDC —●—, TS —□—, G06 —Δ— and experimental (this work) —■—.

8. Tables

TABLE 1 Variation in the unit cell parameters of phases I and II AP with pressure.

Pressure (GPa)	*a* (Å)	*b* (Å)	*c* (Å)	V (Å^3)	wR_p	χ^2
0.01	9.2184(14)	5.8108(9)	7.4504(13)	399.09(7)	0.0805	1.153
0.03	9.2133(13)	5.8075(8)	7.4447(11)	398.34(6)	0.0653	1.317
0.14	9.1868(13)	5.7969(8)	7.4292(11)	395.64(6)	0.0665	1.350
0.30	9.1538(12)	5.7875(8)	7.4038(11)	392.23(6)	0.0613	1.292
0.60	9.0899(11)	5.7621(7)	7.3624(9)	385.62(6)	0.0586	1.276
1.08	9.0054(10)	5.7277(7)	7.3018(9)	376.63(5)	0.0595	1.250
1.60	8.9276(10)	5.6970(7)	7.2472(9)	368.60(6)	0.0745	1.289
2.26	8.8375(10)	5.6634(6)	7.1848(9)	359.60(5)	0.0676	1.396
2.85	8.7699(11)	5.6400(7)	7.1380(10)	353.06(6)	0.0734	1.331
3.49	8.6998(11)	5.6170(7)	7.0908(9)	346.50(5)	0.0655	1.358
3.98	8.6565(21)	5.6022(13)	7.0605(18)	342.40(9)	0.0577	1.475
3.98	7.4580(15)	6.3344(12)	7.1176(17)	336.25(8)	0.0577	1.475
4.60	7.4070(11)	6.3209(9)	7.0734(11)	331.17(6)	0.0793	1.695
5.15	7.3646(11)	6.3051(9)	7.0396(11)	326.88(6)	0.0874	1.757
5.63	7.3276(11)	6.2937(10)	7.0093(12)	323.21(6)	0.0735	1.676
6.15	7.2918(11)	6.2780(9)	6.9815(11)	319.60(5)	0.0712	1.775
6.77	7.2528(13)	6.2587(11)	6.9498(11)	315.47(5)	0.0739	1.800
7.51	7.2074(17)	6.2404(13)	6.9197(12)	311.22(5)	0.0825	1.912
8.13	7.1728(17)	6.2222(14)	6.8909(12)	307.55(5)	0.0884	2.022

TABLE 2 Experimental and calculated 3rd order Birch-Murnaghan equation of state parameters of crystalline AP over the pressure range 0-3.5 GPa.

	Experiment (this work)	*NDC*	*TS*	*G06*
V_0 (Å^3)	399.33(20)	426.87	397.53	382.50
B_0 (GPa)	14.91(25)	11.96	19.91	20.50
B’	7.32(23)	7.12	5.96	7.53

References

[1] Akhavan, J. *The Chemistry of Explosives*; Royal Society of Chemistry, Cambridge, UK, 2nd edition, 2004.

[2] Jacobs, P. W. M.; Whitehead, H. M. *Chem. Rev.* **1969**, *69(4)*, 551.

[3] Politzer, P.; Lane, P. *J. Mol. Strut.* **1998**, *454(2-3)*, 229.

[4] Brill, T. B.; Budenz, B. T. *Progr. Astronaut. Aeronaut.* **2000**, *185*, 3. Eds. Yang, V.; Brill, T. B.; Ren, W. Z. *A.I.A.A.* **2000**, pp 3 – 32.

[5] Stammler, M.; Bruenner, R.S.; Schmidt, W.; Orcutt, D. *Adv. X-ray Anal.* **1966**, *9*, 170.

[6] Bridgman, P. W. *Proc. Amer. Acad. Arts Sci.* **1937**, *72*, 45.

[7] Richter, P. W.; Pistorius, C. F. W. T. *J. Solid State Chem.* **1971**, *3(3)*, 434.

[8] Foltz, M. F.; Maienschein, J. L. *Mater. Lett*. **1995**, *24(6)*, 407.

[9] Sandstrom, F. W.; Persson, P. A.; Olinger, B. *AIP Conference Proceedings* **1994**, *309*, 1409.

[10] Brill, T. B.; Goetz, F. *Papers in Astronaut. Aeronaut.* **1978**, *63*, 3. Eds. Boggs, T. L.; Zinn, B. T. *A.I.A.A.* **1978**, pp 3 – 19.

[11] Yuan, G.; Feng, R.; Gupta, Y. M.; Zimmerman, K. A. *J. Appl. Phys.* **2000**, *88(5)*, 2371.

[12] Winey, J. M.; Gruzdkov, Y. A.; Dreger, Z. A.; Jensen, B. J.; Gupta, Y. M. *J. Appl. Phys.* **2002**, *91(9)*, 5650.

[13] Peiris, S. M.; Pangilinan, G. I.; Russell, T. P. *J. Phys. Chem. A* **2000**, *104(47)*, 11188.

[14] Zhu, W.; Wei, T.; Zhu, W.; Xiao, H. *J. Phys. Chem. A* **2008**, *112(20)*, 4688.

[15] Zhu, W.; Zhang, X.; Zhu, W.; Xiao, H. *Phys. Chem. Chem. Phys.* **2008**, *10(48)*, 7318.

[16] Prask, H. J.; Choi, C. S.; Chesser, N. J.; Rosasco, G. J. *J. Chem Phys.* **1988**, *88(8)*, 5106.

[17] Choi, C. S; Prask, H. J.; Prince, E. *J. Chem Phys.* **1974**, *61(9)*, 3523.

[18] Marshall, W. G.; Francis, D. J. *J. App. Cryst.* **2002**, *35(1)*, 122.

[19] Besson, J. M.; Nelmes, R. J.; Hamel, G.; Loveday, J. S.; Weill, G.; Hull, S. *Physica B* **1992**, *180-181(Pt. B)*, 907.

[20] Larson, A. C.; Von Dreele, R. B. *General Structure Analysis System (GSAS)*; Los Alamos National Laboratory Report, LAUR 86-748, 2000.

[21] Decker, D. L. *J. App. Phys.* **1971**, *42(8)*, 3239.

[22] Merrill, L.; Bassett, W. A. *Rev. Sci. Instrum.* **1974**, *45*, 290.

[23] Piermarini, G. J.; Block, S.; Barnett, J. D.; Forman, R. A. *J. App. Phys.* **1975**, *46(6)*, 2774.

[24] Clark, S. J.; Segall, M. D.; Pickard, C. J.; Hasnip, P. J.; Probert, M. J.; Refson, K.; Payne, M. C. *Z. Krystallogr.* **2005**, *220(5-6)*, 567.

[25] Grimme, S. *J. Comput. Chem.* **2006**, *27(15)*, 1787.

[26] Tkatchenko, A.; Scheffler, M. *Phys. Rev. Lett.* **2009**, *102(7)*, 073005.

[27] Perdew, J. P.; Burke, K.; Ernzerhof, M. *Phys. Rev. Lett.* **1996**, *77(18)*, 3865.

[28] Vanderbilt, D. *Phys. Rev. B* **1990**, *41*, 7892.

[29] Vackar, J.; Hytha, M.; Simunek, A. *Phys. Rev. B* **1998**, *58(19)*, 12712.

[30] Monkhorst, H. J.; Pack, J D. *Phys. Rev. B* **1976**, *13*, 5188.

[31] Fischer, T. H.; Almlof, J. *J. Phys. Chem.* **1992**, *96(24)*, 9768.

[32] Birch, F.; *Phys. Rev.* **1947**, *71*, 809.

[33] Varga, T.; Wilkinson, A. P.; Angel, R. J. *Rev. Sci. Instrum.* **2003**, *74(10)*, 4564.

[34] Bridgman, P. W. *Proc. Amer. Acad. Arts Sci.* **1937**, *71*, 387.

[35] Adams, D. M.; Sharma, S. K. *J. Chem. Soc., Faraday Trans. 2* **1976**, *72(11)*, 2069.

[36] Hegde, B. G.; Rastogi, A.; Damle, R.; Chandramani, R.; Bhat, S. V. *J. Phys.: Condens. Matter* **1997**, *9(15)*, 3219.

[37] Bhat, H. L.; Herley, P. J.; Sheen, D. B.; Sherwood, J. N. *Appl. X-Ray Topogr. Methods Mater. Sci.* **1984**, 401.

[38] Byrd, E. F. C.; Rice, B. M. *J. Phys. Chem. C* **2007**, *111(6)*, 2787.

[39] Conroy, M. W.; Oleynik, I. I.; ZybinS. V.; White, C. T. *J. App. Phys.* **2008**, *104(5)*, 053506.